

FoldA: Computing Partial-Order Alignments Using Directed Net Unfoldings

Douwe Geurtjens¹ and Xixi Lu¹[0000-0002-9844-3330]

Utrecht University, Utrecht, the Netherlands
{d.geurtjens, x.lu}@uu.nl

Abstract. Conformance checking is a fundamental task of process mining, which quantifies the extent to which the observed process executions match a normative process model. The state-of-the-art approaches compute *alignments* by exploring the state space formed by the synchronous product of the process model and the trace. This often leads to state space explosion, particularly when the model exhibits a high degree of choice and concurrency. Moreover, as alignments inherently impose a sequential structure, they fail to fully represent the concurrent behavior present in many real-world processes. To address these limitations, this paper proposes a new technique for computing partial-order alignments *on the fly* using directed Petri net unfoldings, named FoldA. We evaluate our technique on 485 synthetic model-log pairs and compare it against Astar- and Dijkstra-alignments on 13 real-life model-log pairs and 6 benchmark pairs. The results show that our unfolding alignment, although it requires more computation time, generally reduces the number of queued states and provides a more accurate representation of concurrency.

Keywords: Process mining · Conformance checking · Partial-order alignments · Unfolding

1 Introduction

Conformance checking assesses how well real-world executions adhere to a predefined process model [1]. Various methods have been developed for this task, with one of the most widely used being *alignment*-based techniques. These techniques compute an optimal sequence of model-allowed activities that minimizes deviations from a given trace [3]. The alignment-based techniques have been extended in many different ways, such as data-aware [16] and object-centric methods [10].

Current alignment computation relies on exploring the reachability graph of the synchronous product between an input trace and a predefined process model [3]. However, when the model exhibits a high degree of concurrency, the corresponding reachability graph often suffers from state-space explosion due to interleaving semantics, causing it to grow to massively [17]. While alignment techniques use graph search algorithms (e.g., Dijkstra and Astar) and heuristics to reduce the number of explored paths [3], they still select an arbitrary optimal sequential path in the reachability graph and return this as optimal alignment.

Furthermore, these techniques impose a sequential order on the events of a trace and, consequently, on the returned alignment, even when no explicit dependencies exist. This limitation prevents them from accurately capturing the concurrent behavior present in many real-world processes [13]. *Partial-order alignments* were introduced to address this issue and to identify discrepancies in dependencies [13]. The partial-order alignments naturally capture concurrency and dependencies between moves, enabling the identification of much richer deviating patterns while preserving explicit relations between the moves [12,7]. For example, [14] shows their diagnostic value in a healthcare setting.

While partial-order alignments can be used to derive better diagnostics [14,7], their computation *still* relies on sequential exploration of the reachability graph to compute an optimal alignment, which can lead to suboptimal results when dependencies are considered.

Consider the example model and an example of a partial-order trace (also known as a pomset) in Fig. 1. Current alignment techniques consider both $\gamma_1 = \frac{|e_1|e_2|e_3|e_4|}{|t_1|t_2|t_3|t_4|}$ and $\gamma_2 = \frac{|e_1|e_2|e_3|e_4|}{|t_5|t_6|t_7|t_8|}$ as optimal alignments and returns one arbitrarily. If γ_2 is chosen, the method in [13] uses it to compute a partial-order alignment and detects discrepancies in dependencies, for example, A (t_6) is directly followed by B (t_7) in the model, whereas in the trace, A (e_2) and B (e_3) are concurrent. However, the alternative alignment γ_1 , which was not returned, would have produced a better partial-order alignment.

In this paper, we propose a new approach, *unfolding alignments*, leveraging the *directed net unfoldings* technique. Net unfoldings naturally retain concurrency and dependencies in the original net. Pioneered by McMillan [17], the concepts of an adequate order and cut-off events are introduced to mitigate the exponential growth of traditional state-space representations. Built on the idea of using an adequate order, we introduce a cost-based, directed unfolding for computing alignments, allowing us to compute an optimal partial-order run (also called a *configuration*) to the final marking in an *on-the-fly* manner, see Fig. 2.

To evaluate the feasibility and performance of our unfolding alignments, we conducted experiments on 485 synthetic model-log pairs, 13 real-life model-log pairs, and 6 benchmark pairs. Due to the space constraints and the complexity of definitions, this paper focuses on sequential traces, allowing direct comparison with Dijkstra- and Astar-alignments. Nevertheless, the proposed unfolding alignment is also directly applicable to partial-order traces, see the example provided in Appendix A. The remainder of the paper follows a standard structure.

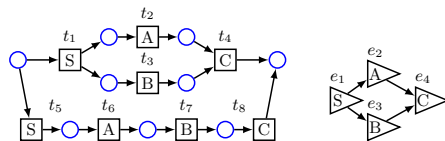


Fig. 1: A Petri net M (left) and a partial-order trace σ (right).

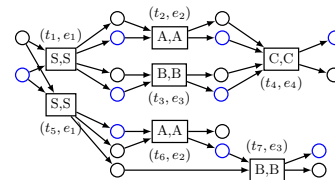


Fig. 2: An (incomplete) prefix unfolding of the synchronous product of M and σ .

2 Related Work

Conformance checking Early conformance checking research focused on defining quantitative metrics to evaluate process discovery algorithms [11]. Replay-based conformance [19] replays a trace on a model, artificially inserting tokens when transitions cannot fire, to identify the problematic places. However, this method struggled with invisible transitions and sometimes introduced behavior not allowed by the model, making it difficult to diagnose deviations [2,3]. To address these issues, the work in [2] introduced alignments, which compute the optimal sequence of pairs of activities permitted by both the model and the trace while minimizing deviations. While alignments improved conformance checking accuracy, their sequential nature posed challenges for highly concurrent processes, as independent events could appear causally dependent [13]. To address this, Lu et al. [13] proposed partial-order alignments, which allow non-sequential behavior by introducing partial-order traces. However, it still relies on the sequential alignment to return a sequential optimal alignment, which may not be the optimal partial-order alignment.

García-Bañuelos et al [7] use net unfolding to obtain prime event structure (PES) for both the input model and the traces. After obtaining these PESs, they compare the two PESs by computing a partially synchronized product. To obtain PESs, they use the ERV unfolding [6] to compute a complete prefix unfolding of the model, which means that it cannot handle unbounded, easy sound nets (i.e., a final marking is reachable). In contrast, our approach first builds the synchronous product of the model and trace, and then unfolds this synchronous product in a directed manner, allowing us to support unbounded, easy sound nets.

Siddiqui et al. [20] also investigate the use of net unfolding for computing partial-order alignments. The idea in this paper was independently developed in 2024 [8] and submitted before [20] became available. There are two key differences: (1) the work in [20] entirely omits the fundamental problem that current alignment-based approaches cannot compute optimal partial-order alignment due to unhandled discrepancies between moves. We highlight this problem explicitly with a concrete example in our problem statement. (2) Our evaluation is significantly broader. While [20] tested only one model type (parallel branches, no loops) and a single real-life event log using only Inductive Miner, we evaluated 485 models with choice, parallelism, and loops, and 13 real-life log-model pairs with Inductive Miner and Split Miner, along with 6 benchmark sets.

Net Unfoldings Petri net unfoldings efficiently represent the state space of a net [17]. The unfolding of a Petri net, potentially infinite, is a Petri net without backward conflict. In such a net, *no two transitions can output to the same place*, enforcing a strict partial order on transitions. In an unfolding, transitions are called *events*, and places *conditions*.

To ensure a compact representation, McMillan [17] introduced *cut-off events*, to stop the unfolding of an event when the marking is already seen in other branches of the unfolding. Later, Esparza et al., [6] identified flaws in the original algorithm, where in some cases, it created an unfolding in which not all reachable

markings were represented. They propose the concept of an *adequate order* on the events of the unfolding, to guarantee that all possible markings are reached and improve computation efficiency. The use of cut-off events also leads to the concept of *finite complete prefixes*, referring to the minimal part of the unfolding that represents all reachable markings.

Bonet et al., [4] refined the approach by generating only the prefix needed to reach a target marking, further enhancing performance. Lastly, Bonet et al., [5] provided an overview of the recent advances in Petri net unfoldings, covering both efficiency and applicability to different Petri net types.

Our approach builds the adequate order and cut-off event concepts from the ERV algorithm [17]. However, unlike ERV, we do not compute a complete prefix unfolding. Instead, we perform a targeted, directed unfolding that prioritizes reaching the final marking as quickly as possible. This is achieved through a best-first search over the events to be appended, while respecting the adequate order. The unfolding process terminates as soon as the final marking is reached.

3 Preliminaries

In this section, we formally define key terms relevant to our work. We assume our readers are familiar with *multiset*, *sequences*, and *Petri nets*; otherwise, we provide definitions in Appendix B for review purposes.

Alignment based conformance checking. We introduce the formal definitions related to event logs, process models, and alignments [3].

Let A be a set of activities. A *trace* $\sigma = \langle e_1, e_2, \dots, e_n \rangle \in A^*$ is a sequence of events where each event is the activity executed. An *event log* $L \subset \mathcal{B}(A)$ is a multiset of traces. A process model N_1 in the form of a Petri Net for the student-housing application process is shown in Fig. 3(a), and an example of trace is $\sigma_1 = \langle \text{MakeBk}, \text{SubmitPD}, \text{AwaitC}, \text{Sign} \rangle$ in an event net form in Fig. 3(b). Currently, only the `MakeBk` transitions are enabled.

Definition 1 (Alignment). Let $N = (P, T, F, i, f)$ denote an easy sound Petri net representing a process model where i is the initial marking and f the final marking. Let σ denote a trace. A valid alignment $\gamma \in ((A \cup \{\gg\}) \times (T \cup \{\gg\}))^*$ is a sequence of moves such that (1) $\pi_1(\gamma) \downarrow_A = \sigma$, i.e., projecting on the first elements of the moves yields the trace, (2) $i \xrightarrow{\pi_2(\gamma) \downarrow_T} f$, i.e., projecting on the second elements yields an occurrence sequence from i to f in N , and (3) $(\gg, \gg) \notin \gamma$. For $a \in A$ and $t \in T$, we call (a, \gg) a log move, (\gg, t) a model move, (a, t) a synchronous move, and (\gg, \gg) an invalid move.

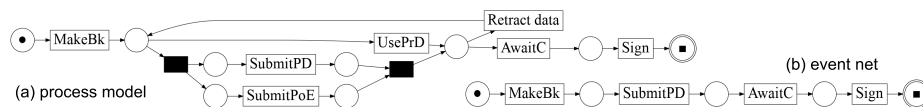


Fig. 3: (a) Process model N_1 in the form of a Petri net and (b) event net N_l for the trace σ_1 .

Definition 2 (Optimal Alignment). Let $\Gamma_{\sigma,N}$ denote the set of all alignments between trace σ and net N . Let $\kappa : (A \cup \{\gg\}) \times (T \cup \{\gg\}) \rightarrow \mathbb{R}^+$ be a cost function for moves. We say that $\gamma \in \Gamma_{\sigma,N}$ is an optimal alignment between σ and N if and only if for all $\gamma' \in \Gamma_{\sigma,N}$, $\kappa(\gamma) \leq \kappa(\gamma')$, where $\kappa(\gamma) = \sum_{(e,t) \in \gamma} \kappa(e,t)$.

Definition 3 (Synchronous product). The synchronous product of two disjoint nets $N_l = (P_l, T_l, F_l, i_l, f_l)$ and $N_m = (P_m, T_m, F_m, i_m, f_m)$ is an easy sound Petri net $sp = N_l \times N_m = (P, T, F, i, f)$, where (1) $P = P_l \cup P_m$; (2) $T = (T_l \times \{\gg\}) \cup (\{\gg\} \times T_m) \cup SM$, where $SM = \{(a,t) \in T_l \times T_m \mid a = t\}$; (3) $F = \bigcup_{(t_l, t_m) \in T} \{(p_l, (t_l, t_m)) \mid (p_l, t_l) \in F_l\} \cup \{(t_l, t_m, p_l) \mid (t_l, p_l) \in F_l\} \cup \{(p_m, (t_l, t_m)) \mid (p_m, t_m) \in F_m\} \cup \{(t_l, t_m, p_m) \mid (t_m, p_m) \in F_m\}$, (4) $i = i_l \cup i_m$, and (5) $f = f_l \cup f_m$.

Figure 4 shows the resulting synchronous product of N_l and N_1 , which is constructed as follows: the transitions present in the model become model moves (colored blue), the transitions in the event net become log moves (colored yellow), and for each pair of transitions that have the same label, we create a synchronous move transition (colored green).

By exploring the reachability graph of the synchronous product using a shortest path algorithm, we derive an optimal alignment $\gamma = \langle (\text{MakeBk}, \text{MakeBk}), (\gg, \text{SubmitPoE}), (\text{SubmitPD}, \text{SubmitPD}), (\text{AwaitC}, \text{AwaitC}), (\text{Sign}, \text{Sign}) \rangle$.

Definition 4 (Partial Order Alignment). Let $sp = (P, T, F, i, f) = N_l \times N_m$ be a synchronous product of process model N_m and event net N_l . A partial-order alignment δ is a partial-order over the moves such that (1), (2) and (3) from Definition 1 are respected.

Informally, we can say that events in a partial-order trace can be “tied” in their execution, rather than strictly sequential as in a conventional trace σ . The same holds for a partial-order alignment δ when compared to a regular alignment γ . In both cases, the only difference with their conventional counterpart is that the order is partial, rather than total.

Net Unfoldings Here, we introduce the key definitions from [6] to understand the process of unfolding a Petri Net, revisiting our running example. By “unfolding” a net N , we obtain a so-called branching process β of N , which is a labeled occurrence net. Given a net, we say x causes y , i.e., $x < y$, if there is a directed path from x to y ; we say x is in conflict with y , i.e., $x \# y$, if x and y originate from the same place but follow diverging paths; and x is concurrent with y , i.e., $x \parallel y$, if x and y are neither casually related nor in conflict.

Definition 5 (Occurrence net). An occurrence net is a net $O = (B, E, G)$ in which B denotes a set of conditions, E denotes a set of events, and G denotes

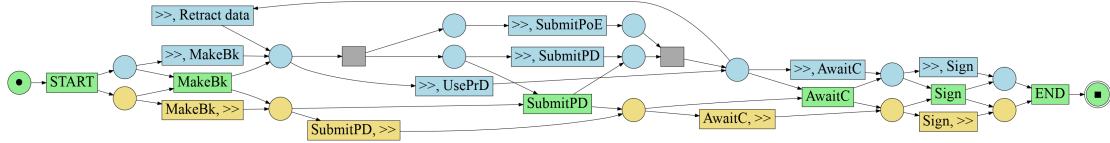


Fig. 4: The synchronous product between N_1 and σ_1 in Fig. 3.

the causal relations such that: (1) $|\bullet b| \leq 1$ for every $b \in B$, meaning every condition has at most one incoming event; (2) O is acyclic; (3) O is finitely preceded, i.e., for all $o \in O$, o has a finite number of causal predecessors; (4) No element is in conflict with itself.

Definition 6 (Branching process). A branching process β of a net $N = (P, T, F, i, f)$ is a labeled occurrence net $(O, p) = (B, E, G, p)$ (possibly infinite) where the labeling function $p : (E \rightarrow T) \cup (B \rightarrow P)$ satisfies the following properties: (1) for every $e \in E$, the restriction of p to $\bullet e$ is a bijection between $\bullet e$ in N and $\bullet p(e)$ in β , and similar for e^\bullet and $p(e)^\bullet$; (2) β starts with i , i.e., $p(\text{Min}(O)) = i$ where $\text{Min}(O) = \{b \in B \mid \bullet b = \emptyset\}$; (3) for every $e_1, e_2 \in E$, if $\bullet e_1 = \bullet e_2$ then $e_1 = e_2$ (i.e., β does not duplicate events).

Figure 5 shows a branching process of the net in Fig. 3. This unfolding has deliberately been cut off at an arbitrary point, as the full unfolding would be infinite. For the basic algorithm to construct an unfolding, we refer to [17].

Definition 7 (Configuration, Cut). A configuration $C \subseteq E$ of a branching process $\beta = (O, p) = (B, E, G, p)$ is a set of events such that (1) C is causally closed, i.e., $\forall e \in C, \forall e' < e : e' \in C$ and (2) C is conflict-free, i.e., $\forall e, e' \in C : \neg(e\#e')$. We use $\text{Cut}(C)$ to denote the cut of a configuration, which is a set of conditions in β that represents the marking of the net after firing the events in the configurations, i.e., $\text{Cut}(C) = (\text{Min}(O) \cup C^\bullet) \setminus \bullet C$. We use the marking of configuration $\text{Mark}(C) = p(\text{Cut}(C))$ to refer to the marking in the original net. We define $\uparrow C$ as the pair (O', p') where O' is the unique subnet of O whose set of nodes is $\{x \mid x \notin C \cup \bullet C \wedge \forall y \in C : \neg(x\#y)\}$ and p' is the restriction of p to the nodes of O' .

Figure 5 highlights the configuration of $\{\text{MakeBk}, \text{SubmitPD}, \text{SubmitPoE}\}$ is marked in green, with its corresponding cut being marked in blue. The notion $\uparrow C$ denotes the future part of β that is possible after C , excluding anything that has already occurred or is in conflict with C .

Definition 8 (Extension). Given a configuration C , its extension $C \oplus E$ is defined as $C \cup E$ while $C \cap E = \emptyset$.

In Figure 5, a possible extension of the marked configuration is the event representing the silent transition whose preset is the set of conditions marked in blue. The event marked in red cannot be added to this configuration, as it would violate conflict-freeness.

Definition 9 (Configuration Isomorphism). Let C_1 and C_2 be two configurations that lead to the same marking, i.e. $\text{Mark}(C_1) = \text{Mark}(C_2)$, then I_1^2 is

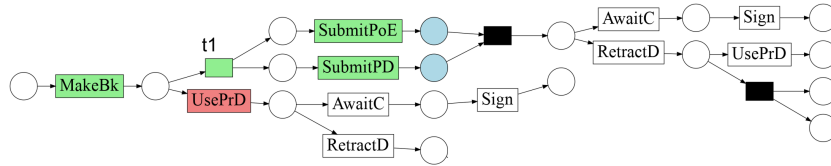


Fig. 5: A prefix of the unfolding of Figure 3, with color coding of a configuration.

the isomorphism of $\uparrow C_1$ and $\uparrow C_2$. This isomorphism induces a mapping from the finite extensions of C_1 onto the finite extensions of C_2 : it maps $C_1 \oplus E$ onto $C_2 \oplus I_1^2(E)$.

Definition 10 (Local configuration). Let $\beta = (B, E, G, l)$ be a branching process of the model sp . The local configuration of an event $e \in E$, denoted by $[e]$, is the set of events e' such that $e' \leq e$.

For example, the local configuration $[\text{SubmitPD}] = \{\text{MakeBk}, \text{SubmitPD}, t_1\}$ in Fig. 5.

Definition 11 (Local configuration cost). Given a branching process $\beta = (B, E, F, p)$ and its associated net $N = (P, T, F, i, f)$, we define a cost function $Z([e], \zeta)$ for a local configuration $[e]$ as follows: $\sum_{e \in [e]} \zeta(p(e))$, where $\zeta(t)$ assigns a numerical cost to each $t \in T$.

Definition 12 (Adequate order). A partial order \prec on the finite configurations of the unfolding of a net N is an adequate order if:

- \prec is well-founded,
- $C_1 \subset C_2$ implies $C_1 \prec C_2$, and
- \prec is preserved by finite extensions; if $C_1 \prec C_2$ and $\text{Mark}(C_1) = \text{Mark}(C_2)$, then the isomorphism I_1^2 from above satisfies $C_1 \oplus E \prec C_2 \oplus I_1^2(E)$ for all finite extensions $C_1 \oplus E$ of C_1 .

Definition 13 (Cut-off event). Let \prec be an adequate order on the configurations of the unfolding of a net N . Let β be a prefix of the unfolding containing an event e . The event e is a cut-off event of β (with respect to \prec) if β contains a local configuration $[e']$ such that (1) $\text{Mark}([e]) = \text{Mark}([e'])$, and (2) $[e'] \prec [e]$.

As previously stated, the unfolding of a Petri net can be infinite due to loops or unbounded behavior. To address this, cut-off events are used to terminate parts of the unfolding when a previously encountered marking is reached again. This avoids redundant exploration of equivalent behavior. By applying this mechanism, one can construct a *finite complete prefix*, which is a finite branching process that still captures all reachable markings of the original Petri net, if it is bounded.

4 Approach

This section presents our approach for computing partial-order alignments using net unfolding. As no prior work has tackled alignments via Petri net unfoldings, we introduce an algorithm for this task and propose a few optimizations to enhance performance. Figure 6 shows an overview of the approach.

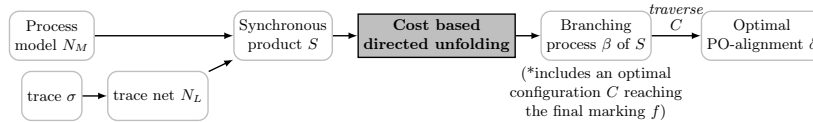


Fig. 6: An overview of the unfolding alignment approach

4.1 The Directed-Unfolding Algorithm

In essence, the algorithm operates as follows. It begins by constructing the synchronous product $sp = (P, T, F, im, fm)$ of the model net N_m and the event net N_l . It then unfolds sp in a directed, cost-based manner to create a branching process $\beta = (B, E, G, p)$, terminating once the final marking fm is reached in some configuration, i.e., $\exists C \in \beta$ such that $Mark(C) = fm$. To simplify this check, we added a dummy end event to the synchronous product, allowing us to use the local configuration of this event instead. Thus, the stopping condition becomes: $\exists x \in \beta$ such that $Mark([x]) = fm$. The corresponding configuration $[x]$ defines the optimal partial-order alignment δ . With this idea, Algorithm 1 presents the pseudocode for computing an optimal partial-order alignment via directed unfolding, built on the idea of cut-off events and an adequate order [6].

Algorithm 1: A pseudocode algorithm for computing partial-order alignments through directed unfolding

Data: A net N_m with a reachable final marking, an event net N_l
Result: An optimal partial-order alignment δ

```

1   $cost \leftarrow \zeta(t) = \begin{cases} 0 & \text{if } t \text{ is synchronous} \\ 1 & \text{if } t \text{ is model or log;} \\ 0.0001 & \text{if } t \text{ is silent} \end{cases}$ 
2   $sp = (P, T, F, im, fm) \leftarrow N_l \times N_m$ ; /* Create a synchronous product  $sp$ , with its
   initial marking  $im$  and final marking  $fm$  */
3   $\beta \leftarrow InitializeBranchingProcess(sp, im)$ ;
4   $pe \leftarrow PossibleExtensions(\beta)$ ;
5   $cutoff \leftarrow \emptyset$ ;
6   $\delta \leftarrow \emptyset$ ;
7  while  $pe \neq \emptyset$  do
8    choose an event  $e = (t, X)$  in  $pe$  such that  $Z([e], \zeta)$  is minimal;
9    if  $[e] \cap cutoff = \emptyset$  then
10      $\beta \leftarrow \beta \cup e$ ;
11      $\beta \leftarrow \beta \cup \{(s', e) \mid s \in p(e)^\bullet, p(s') \leftarrow s\}$ ; /* for each place  $s$  in the postset of
   the transition corresponding to  $e$ , create a condition  $s'$  and add it to the
   branching process */
12     if  $\exists x \in \beta; Mark([x]) = fm$ ; /* Reached the final marking */
13     then
14        $\delta \leftarrow [x]$ ; /* Update optimal alignment */
15       BREAK the while loop.
16      $pe \leftarrow PossibleExtensions(\beta)$ ;
17     if  $e$  is a cut-off event of  $\beta$  then
18        $cutoff \leftarrow cutoff \cup \{e\}$ ;
19    $pe \leftarrow pe \setminus e$ ;
20 return  $\delta$ ; /* Return this optimal alignment */

```

We begin by computing sp and initializing β using the initial marking im of sp , adding a *condition* to β for each place in im (see Lines 1-3). A *condition* (s, e) consists of a place in sp and a pointer to its input event, while an *event* (t, X) consists of a transition t in sp and a set X of input conditions. In pseudocode, conditions are represented as (s, e) or (s, \emptyset) , and events as (t, X) .

After initializing the branching process β , we begin unfolding sp by firing enabled transitions (as possible extensions, see Line 4), adding each as a new event in β , and appending its post-set as new conditions. The transition selection must follow the adequate order to ensure correctness and optimality during directed unfolding.

We define the adequate order \prec using the cost function $Z([e], \zeta)$ of a local configuration $[e]$, based on a predefined cost function ζ . We use the standard cost

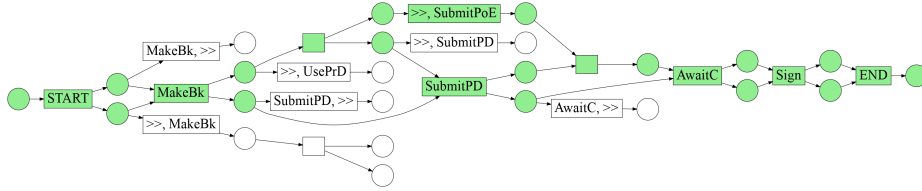


Fig. 7: The branching process constructed by Algorithm 1 on the synchronous product in 4. The optimal partial-order alignment is highlighted in green.

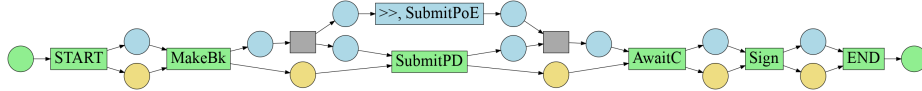


Fig. 8: The optimal partial-order alignment as an occurrence net.

function for ζ , as listed in Algorithm 1. Thus, $e \prec e'$ if and only if $Z([e], \zeta) \leq Z([e'], \zeta)$. To break any ties and maintain the adequate order \prec , each event e is assigned a unique numerical identifier using Python's built-in `id()` function¹, i.e., if $Z([e], \zeta) = Z([e'], \zeta)$, we order the events by $id(e) < id(e')$.

We iteratively append the *best* possible extension e to β (see Lines 7-11), check whether the final marking is represented (see Lines 12-15), and, if not, continue with computing new possible extensions and the next *best* extension (see Lines 16-20). Once the final marking is reached, we return the corresponding configuration, which defines an optimal alignment guaranteed by \prec . Figure 7 illustrates a directed unfolding of sp from Fig. 4, and Figure 8 shows the resulting partial-order alignment.

Theorem 1 (Correctness of Unfolding Alignment). *Given a Petri net N_m and an event net N_l , let δ be the alignment returned by Algorithm 1, which is defined by an optimal configuration $[e]$ in the branching process β of the synchronous product $sp = N_m \times N_l$. Then, δ is a valid, optimal partial-order alignment. Specifically: (1) $\delta \subseteq \beta$ corresponds to a valid firing sequence in sp from its initial marking im to final marking fm . (2) If a valid alignment exists, the unfolding contains it, and the algorithm will find it. (3) The alignment δ minimizes the cost $Z([e], \zeta)$ among all valid alignments. (4) The algorithm terminates.*

Proof. For (1), all added events correspond to enabled transitions, preserving soundness (guaranteed by the definition of a branching process). For (2) and (4), by Theorem 4.3.4 and Lemma 4.4.1 in [3], the final marking fm is reachable in sp , thus, also reachable in β . Once it is reached, our algorithm terminates. For (3), the ERV unfolding algorithm guarantees that β contains at least one path to fm . Our algorithm explores configurations in order of increasing cost guaranteed by \prec and selects the first reaching fm , ensuring optimality.

To enhance performance, we implement a few optimizations. The set of possible extensions (pe in Algorithm 1) is implemented as a priority queue, ensuring efficient selection of the lowest-cost extensions. Moreover, we store events indexed

¹ <https://docs.python.org/3/library/functions.html#id>

by their marking, which simplifies cut-off event detection. Additionally, each event retains its local configuration and cost, enabling faster cost computations for new extensions and quick identification of cut-off events. We refer to this algorithm as FoldA_n .

4.2 Using Heuristics

In the previous section, we defined the adequate order \prec using the cost function $Z([e], \zeta)$, following a Dijkstra approach. To reduce backtracking, we present a heuristic function $h_{sp}(\text{Mark}([e]))$, which estimates a lower bound on the remaining cost for an extension e to reach the final marking fm , adopting an A* approach. This heuristic is computed by solving the marking equation of the synchronous product for minimum cost, as proposed in [3]. The new adequate order \prec is then defined using $Z([e], \zeta) + h_{sp}(\text{Mark}([e]))$. We omit the subscript sp when the context is clear. While Theorems 4.4.8 and 4.4.9 in [3] prove that this heuristic yields a valid lower bound for traditional alignment computation, its permissibility in directed unfolding has not been established [4]. We now prove that the heuristic remains valid in our unfolding-based setting. We first show that the computed heuristic value there corresponds with a certain event e in β .

Theorem 2. *Given an easy sound Petri net N and its reachability graph $RG(N)$, a complete, finite prefix $\beta = (B, E, G, p)$ of N , and the marking-equation based heuristic function h , then $\forall e \in E, \exists s \in RG(N) : h(\text{Mark}([e])) = h(s)$.*

This follows trivially from the definition of a branching process. Since each $[e]$ represents a valid firing sequence leading to a reachable marking s , and h depends solely on the marking, the heuristic values must match.

Since the heuristic $h(m)$ estimates the minimal cost from a marking m to fm , it preserves alignment optimality. We update Line 8 of Algorithm 1 to select the next event e that minimize $\min_{e \in pe} Z([e], \zeta) + h(\text{Mark}([e]))$. Now, we show that the adequate order \prec is preserved [4]. The first condition (\prec is well-founded) holds trivially, since cost and heuristic values are non-negative, ensuring a minimal cost always exists. The third condition (\prec is preserved by finite extensions) is also straightforward. Since the heuristic value for any two extensions with the same marking is the same, the adequate order remains unchanged. We now prove the second condition, namely that $C_1 \subset C_2$ implies $C_1 \prec C_2$.

Theorem 3. *Let e_1 and e_2 be two events such that $[e_1] \subset [e_2]$, with a cost function $Z([e], \zeta)$, and the heuristic function h . Then, $[e_1] \prec [e_2]$, i.e., $Z([e_1], \zeta) + h(\text{Mark}([e_1])) \leq Z([e_2], \zeta) + h(\text{Mark}([e_2]))$ holds.*

Proof. Assume, for contradiction, that $Z([e_1], \zeta) + h(\text{Mark}([e_1])) > Z([e_2], \zeta) + h(\text{Mark}([e_2]))$. Let $E_d = [e_2] \setminus [e_1]$, i.e., $[e_1] \cup E_d = [e_2]$. This implies that $h(\text{Mark}([e_1])) > Z(E_d, \zeta) + h(\text{Mark}([e_2]))$. This implies that there exists a path from $\text{Mark}([e_1])$ to the final marking fm via E_d and $\text{Mark}([e_2])$ that is cheaper than the heuristic from $\text{Mark}([e_1])$ alone. This contradicts the assumption that h is a lower bound. Therefore, the inequality must hold, and thus $[e_1] \prec [e_2]$.

Thus, we have shown that the heuristic function is valid for use in directed unfoldings and that \prec holds. We refer to this heuristic-enhanced version as FoldA_h . We compare FoldA_n and FoldA_h in our evaluation.

5 Evaluation

This section outlines the evaluation setup for the proposed approach. We first examine the feasibility of our approach. Then, Experiment 1 examines the impact of *model structure* and the *placement of deviations* on unfolding alignment performance. We investigate three model constructs, namely concurrency, choice, and loops. Experiment 2 evaluates unfolding alignment performance against Dijkstra and Astar based alignments using 7 real-world and 6 benchmark logs.

To assess performance, we measure the following metrics for each alignment: elapsed time (ET), number of queued states (#QS), and number of visited states (#VS). To determine how certain attributes of the input data affect performance, we also measure cost, trace length, and number of transitions in the synchronous product (#SPT).

All experiments were performed on a Lenovo IdeaPad 5 equipped with an AMD Ryzen 7 5700U CPU with a clock speed of 1.8 GHz (up to 4.3 GHz turbo) and 16GiB of memory. The code was executed using Python 3.12.0, on Ubuntu 22.04.4 LTS 64-bit. For the baseline techniques, we use PM4PY’s implementations of Dijkstra (no heuristic) and Astar (with heuristic) alignments. Since our implementation is also built upon PM4Py, this allows us to control for programming language, preprocessing, and data structure differences. The source code is publicly available on GitHub² [9].

Feasibility. We began by testing the feasibility of our approach using the real-life healthcare dataset Sepsis (SP) [15] and a *perfectly fitting* model discovered using the inductive miner in PM4PY. The log contains 1050 traces, with lengths ranging from 3 to 185 (avg. 14.49). We evaluated the *naive* unfolding alignments (FoldA_n), i.e., without heuristics, against Dijkstra and A*. All three techniques produced optimal alignments (identical costs). Interestingly, FoldA_n achieved a lower median elapsed time (0.023s) compared to Dijkstra (7.425s) and Astar (0.614s), along with fewer queued and visited states. However, we observe that FoldA_n has extreme outliers, with a maximum elapsed time of 2702 seconds, far exceeding Astar (25s) and Dijkstra (87s). This is also reflected in the mean of elapsed time, where FoldA_n is much higher than Astar (5.43s vs 0.69s).

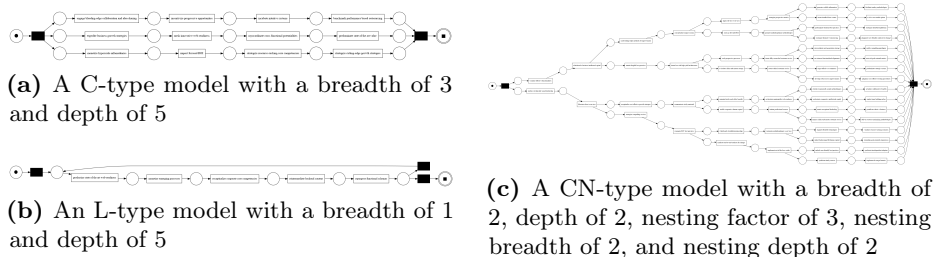
5.1 Experiment 1 - Impact of Model Structure and Deviations

Setup Here, we compare FoldA_n and FoldA_h. To assess the impact of concurrency, choice, and loops, we created artificial process models that isolate each construct. Each model type is defined by breadth (number of branches), depth (branch length), and for concurrency/choice models, nestedness (how often a construct is repeated, which may exponentially increase model size). Fig. 9 illustrates representative examples, and Table 1 outlines parameter ranges. Each model was assigned unique transition labels, and 50 random traces were generated per model, resulting in 24,250 traces across 485 models.

² <https://github.com/DouweGeurtjens/unfolding-alignments>

Table 1: A taxonomy of the artificial datasets used in Experiment 1.

Model type	Construct	Breadth (Min-Max)	Depth (Min-Max)	Nesting Factor (Min-Max)	Nesting Breadth (Min-Max)	Nesting Depth (Min-Max)
C	Concurrency	2-12	1-15	NA	NA	NA
E	Choice	2-15	1-15	NA	NA	NA
CN	Concurrency	2-2	1-5	1-5	2-2	1-5
EN	Choice	2-2	1-5	1-5	2-2	1-5
L	Loop	1-1	1-5	NA	NA	NA

**Fig. 9:** Examples of the artificially generated models used in experiment 1.

To simulate deviations, we systematically removed one event per trace at the start, middle, or end. We decided not to insert or replace the events due to the combinatorial explosion of options. Each alignment computation was limited to 100 seconds per trace.

Results Fig. 10 displays scatterplots showing the relationship between synchronous product transitions and visited states. The relationship is generally linear across model types and deviation placements. For FoldA_n , coefficients vary with deviation placement, whereas for FoldA_h , coefficients remain stable.

Fig. 11 depicts visited states versus elapsed time. Without heuristics (FoldA_n), no clear trend emerges once deviations are introduced. With heuristics (FoldA_h), the relationship appears polynomial or exponential. The differing coefficients between the model types indicate their influence on FoldA_n and FoldA_h .

Impact of Deviations and Heuristics The top row in Fig. 10 shows that for FoldA_n , the number of visited states increases as the position of deviations moves toward the end of the trace. In comparison, the bottom row shows that for FoldA_h , visited states remain consistent regardless of the positioning of deviations, indicating the heuristic helps control state-space explosion.

However, heuristics do not eliminate backtracking, and real-world performance may vary. Although the results show a linear relationship between synchronous product size and visited states, there seems to be a polynomial or exponential relation between visited states and elapsed time (Fig. 11). Additionally, while heuristics mitigate the impact of deviations on time, it comes with a cost: for non-deviation cases, heuristics increase maximum computation time from 2.98s to 70.44s.

Deviation Placement And Backtracking Backtracking is an inherent aspect of directed search, where the algorithm prioritizes lower-cost extensions, even if they are not immediately adjacent to the end state. The nonlinear relationship as observed in Fig. 11 confirms this challenge. Unlike traditional methods, unfolding

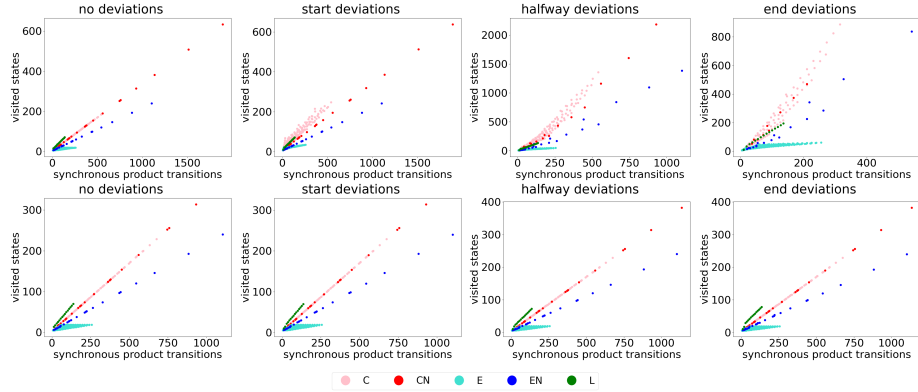


Fig. 10: #VS vs #SPT, across model types and deviation placements, comparing FoldA_n (top four) with FoldA_h (bottom four).

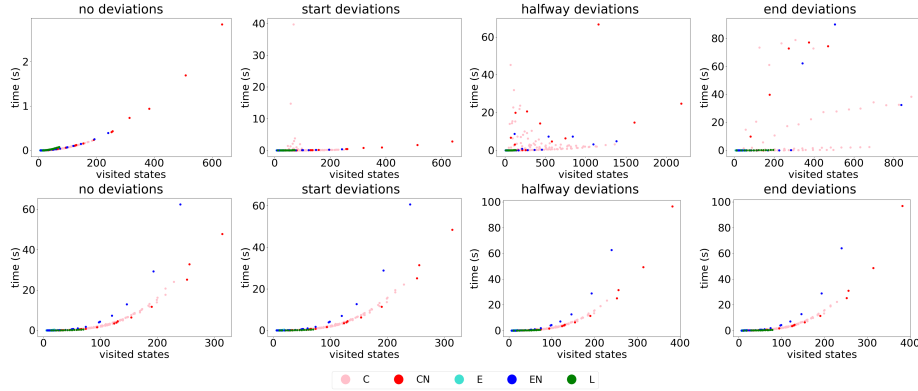


Fig. 11: Elapsed time per #VS across model types and deviation placements, comparing FoldA_n (top four) versus FoldA_h (bottom four).

alignments rely on a branching process, which requires the checking of multiple condition sets per transition to determine whether the transition can be a valid extension. As the branching process increases in complexity, the computational overhead of checking the condition sets rises exponentially, which likely explains the observed nonlinear relationship between visited states and elapsed time.

Impact Of Process Constructs Fig. 11 indicates that EN-type models (nested choice) exhibit the fastest increase in elapsed time. Furthermore, when heuristics are applied, C and CN-type models display similar performance, suggesting that concurrency is managed more effectively than choice constructs. The introduction of choice constructs increases the number of branching configurations, thereby raising computational costs and degrading overall performance.

The findings highlight the significant impact of deviation placement on computational performance when no heuristics are used. While the number of visited states scales linearly with synchronous product size, elapsed time follows a poly-

nomial or exponential relation when heuristics are used. Process models with choice and nested choice constructs impose the highest computational burden.

5.2 Experiment 2 - Comprehensive Performance Comparison

This experiment evaluates FoldA_h using 19 log-model pairs. For the 7 real-world event logs from various sectors such as healthcare and banking, for each of these logs, we discovered a normative process model using two algorithms: Inductive Miner (IM) with noise thresholds of 0.2 (except 0.5 for SP, as lower values did not result in a deviation in every trace) and Split Miner (SM) with default settings, (excluding the BPIC19 log, where SM did not return a model). Additionally, we also include 6 artificial event logs (ITL), which were used as a benchmark for large-scale conformance checking [18]. For the ITL logs, we use the predefined reference models (275-429 transitions) [18]. An overview is listed in Table 2.

Due to the dataset size, 1000 traces were randomly sampled from BPIC12, BPIC13, BPIC17, BPIC19, HB, and TR. Alignments were computed with a 100-second timeout per trace to ensure the feasibility of the experiment.

Results Table 2 lists that for FoldA_h , the median of the elapsed time is much lower than the mean, with the exception of ITL prBm6, TR, and TR_SPLIT. This difference indicates a possible long-tailed elapsed time distribution. We highlight ITL prCm6 and BPIC17, which very clearly exhibit this effect. FoldA_h achieved sub-second mean computational times on 10 out of 13 real-life datasets (i.e., SP, SP_SPLIT, BPIC19, HB, HB_SPLIT, BPIC13, BPIC13_SPLIT, TR, TR_SPLIT, and BPIC12_SPLIT). For the remaining datasets, mean times ranged from 1.23 to 46.50 seconds, with the highest elapsed times observed in BPIC12, BPIC17, BPIC17_SPLIT, and the artificially generated ITL datasets.

When comparing performance, Astar consistently outperformed FoldA_h in elapsed time, requiring 71.45% to 99.11% less time across all completed datasets. However, Astar queued more states in 15 out of 19 datasets, ranging from 22.73% to 578.80% more while visiting fewer states in 16 out of 19 cases (0.80% to 59.89% fewer). Dijkstra also showed faster execution on 13 out of 19 log-model pairs, reducing the elapsed time by 38.64% to 99.27%. However, it queued significantly more states across all datasets, with increases ranging from 1.89% to 118,318.48%, and visited more states in 14 out of 19 cases.

Looking beyond aggregates, FoldA_h generally struggles with larger models and traces. It also suffers extreme outliers, often reaching time-outs on datasets that pose no problem to either Astar or Dijkstra. This is especially noticeable in the ITL prCm6 and BPIC17 datasets, where FoldA_h only complete 328/500 and 697/1000 traces, compared to the 500/500 and 1000/1000 for Astar and Dijkstra.

Even in datasets without time-outs, FoldA_h exhibited significantly higher maximum elapsed times. For example, on SP and SP_SPLIT, the mean times were 0.204 and 0.895 seconds, but the maximums reached 93.447 and 99.987 seconds, respectively. In contrast, the maximums required by Astar were 1.495 and 53.633 seconds, while Dijkstra needed only 2.820 and 4.056 seconds.

Fig. 12(a) shows the effect of the number of transitions in the synchronous product on the visited states across datasets, demonstrating significant variations

Table 2: Elapsed times and queued and visited states of FoldA_h, Astar, and Dijkstra on each dataset and the corresponding process model. Note that the performance is calculated on the finished traces.

Log-model pair	Finished/total				#SPT			Elapsed time (sec.)						Queued states			Visited states		
	FoldA _h	Astar	Dijkstra	Total	FoldA _h	Astar	Dijkstra	FoldA _h		Astar		Dijkstra		FoldA _h	Astar	Dijkstra	FoldA _h	Astar	Dijkstra
	Median	Mean	Median	Mean	Median	Mean	Median	Mean	Median	Mean	Median	Mean	Median	Mean	Median	Mean	Median	Mean	Median
BPIC12	799	1000	1000	1000	92	106	106	0.102	2.014	0.015	1.440	0.633	1.795	274	14016	86252	144	3573	12867
BPIC12_SPLIT	827	1000	1000	1000	64	77	77	0.013	0.954	0.004	0.037	0.007	0.011	156	206	680	87	115	375
BPIC13	650	1000	1000	1000	31	31	31	0.013	0.039	0.002	0.003	0.002	0.002	57	88	161	31	32	62
BPIC13_SPLIT	998	1000	1000	1000	25	25	25	0.008	0.139	0.002	0.004	0.001	0.002	84	44	86	66	28	55
BPIC17	679	999	999	1000	135	151	151	3.135	15.607	0.941	2.349	0.237	0.524	2043	7784	21622	1346	2987	6946
BPIC17_SPLIT	972	1000	1000	1000	115	117	117	0.198	1.230	0.010	0.021	0.020	0.026	233	162	1486	134	67	909
BPIC19	986	1000	1000	1000	102	103	103	0.512	0.777	0.093	0.265	0.732	1.839	585	2577	70655	220	476	9476
HB	1000	1000	1000	1000	67	67	67	0.049	0.055	0.004	0.006	0.003	0.003	74	96	229	33	29	78
HB_SPLIT	1000	1000	1000	1000	41	41	41	0.015	0.077	0.002	0.002	0.001	0.002	32	28	54	15	11	26
SP	1048	1050	1050	1050	55	56	56	0.040	0.204	0.007	0.012	0.096	0.128	75	177	5425	39	32	1465
SP_SPLIT	1022	1050	1050	1050	53	55	55	0.041	0.895	0.007	0.150	0.110	0.141	122	492	6919	65	159	1974
TR	1000	1000	1000	1000	35	35	35	0.015	0.012	0.002	0.002	0.057	0.041	27	55	2412	14	12	390
TR_SPLIT	1000	1000	1000	1000	26	26	26	0.007	0.006	0.001	0.001	0.001	0.001	17	17	36	8	6	18
ITL prAm6	1200	1200	1200	1200	428	428	428	1.522	2.264	0.036	0.136	1.567	4.790	146	187	173193	62	58	34059
ITL prBm6	1200	1200	1200	1200	402	402	402	1.947	1.926	0.034	0.053	0.031	0.047	137	169	169	43	41	41
ITL prCm6	328	500	500	500	395	405	405	12.960	18.694	2.049	4.833	0.961	0.995	991	3794	63766	743	1614	18855
ITL prDm6	732	732	0	1200	919	919	-	45.656	46.503	0.957	1.478	-	-	768	5216	-	264	257	-
ITL prEm6	1200	1200	0	1200	475	475	-	5.456	5.493	0.115	0.148	-	-	323	1000	-	105	104	-
ITL prFm6	686	686	0	1200	783	783	-	30.517	30.641	0.395	0.500	-	-	740	2894	-	247	245	-

in visited states for a given synchronous product size and dataset. This variation can also be seen for the logarithm of elapsed time in Fig. 12(b). BPIC17 and ITL prCm6 stand out in particular.

Fig. 12(c) depicts the relationship between visited states and elapsed time, with the log-log plot suggesting a polynomial correlation. Similarly, Fig. 12(d) shows a linear relationship between synchronous product size and the logarithm of elapsed time, indicating an exponential dependence between them. Note that in both cases the precise relationship appears to be specific to a given model, indicating that, on their own, these metrics do not describe the performance characteristics generally. Additionally, this confirms that the previously assumed linear relationship between visited states and synchronous product size does not hold in more complex datasets. Fig. 12(d) examines cost in relation to elapsed time but reveals no clear patterns due to high variability.

Overall, these findings indicate that the outliers cannot be attributed entirely to a single metric. This tracks with the findings in Experiment 1, which suggest that the interplay between model complexity and the efficacy of the directed search drives performance degradation through the additional costs incurred by backtracking when compared to traditional approaches.

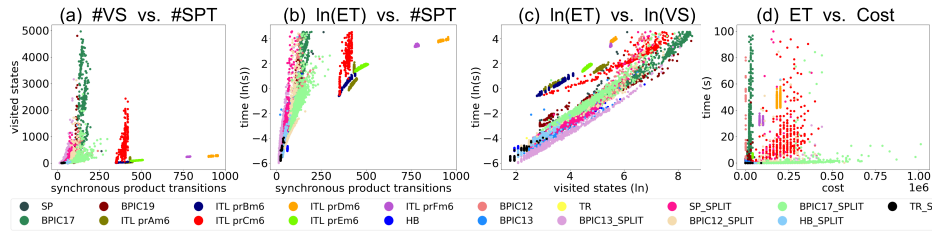


Fig. 12: Correlation analysis of visited states, transitions, and elapsed time.

Regression analysis We applied linear regression to predict the elapsed time of FoldA_h , examining whether time complexity can be estimated using pre-computation metrics and if additional post-computation metrics improve the prediction. We use the $\ln(ET)$ as our dependent variable. We selected the independent variables using correlation analysis and recursive feature elimination. The first regression, using only pre-computation metrics, yields a statistically significant model with an adjusted R^2 of 0.770. The estimated regression coefficients for each independent variable are: $\#SPT$ (2.891), choice factor (0.715), and concurrency factor (-0.161). We define the choice factor as the average number of outgoing arcs per place in the model, and the concurrency factor as the average outgoing arcs per transition in the model. The second regression, incorporating post-computation metrics, achieves a stronger fit with an adjusted R^2 of 0.970. Its coefficients are: $\#SPT$ (1.288), visited states (\ln) (-0.399), and queued states (\ln) (2.271). These findings, particularly those of the second regression, provide additional context for the performance characteristics of FoldA_h . Firstly, it confirms the impact model size has on performance. Secondly, it explains the impact of the directed search component via the relation between the coefficient of visited states and queued states. In essence, the negative coefficient for visited states results in lower elapsed times when a greater portion of the states that were queued, are also visited. It thereby proxies the efficiency of the directed search component of the algorithm.

6 Conclusion

This paper introduced a new approach for computing optimal partial-order alignments using Petri net unfoldings. We designed and implemented an algorithm that integrates Petri net unfoldings with a directed search, evaluating its performance across different process constructs and comparing it to traditional alignment methods.

Our findings indicate that unfolding alignments are computationally viable but sensitive to model structure and deviation placement, with choice constructs and late deviations leading to performance degradation. We mitigated this with a heuristic-guided search, improving efficiency. While our approach underperforms compared to AStar and Dijkstra in terms of execution time, it does effectively reduce the number of queued states. Moreover, this approach retains dependencies between moves during the unfolding, which allows for designing more advanced cost functions in the future, improving diagnostic capabilities beyond traditional sequential alignment approaches. It can also be easily adapted to incremental and parallel alignment computing. Future research may also focus on optimizing performance by designing heuristics tailored towards branching processes.

Acknowledgement We thank Artem Polyvyanyy, Dirk Fahland, and Thomas Chatain for their invaluable discussion in 2017 on the previous idea that inspired this idea.

References

1. van der Aalst, W.M.P.: Process mining: A 360 degree overview. In: *Process Mining Handbook, Lecture Notes in Business Information Processing*, vol. 448, pp. 3–34. Springer (2022)
2. van der Aalst, W.M.P., Adriansyah, A., van Dongen, B.F.: Replaying history on process models for conformance checking and performance analysis. *WIREs Data Mining Knowl. Discov.* **2**(2), 182–192 (2012)
3. Adriansyah, A.: *Aligning observed and modeled behavior* (2014)
4. Bonet, B., Haslum, P., Hickmott, S.L., Thiébaux, S.: Directed unfolding of petri nets. vol. 1, pp. 172–198 (2008)
5. Bonet, B., Haslum, P., Khomenko, V., Thiébaux, S., Vogler, W.: Recent advances in unfolding technique. *Theoretical Computer Science* **551**, 84–101 (2014)
6. Esparza, J., Römer, S., Vogler, W.: An improvement of mcmillan’s unfolding algorithm. In: *TACAS. LNCS*, vol. 1055, pp. 87–106. Springer (1996)
7. García-Bañuelos, L., van Beest, N., Dumas, M., Rosa, M.L., Mertens, W.: Complete and interpretable conformance checking of business processes. *IEEE Trans. Software Eng.* **44**(3), 262–290 (2018)
8. Geurtjens, D.: *Computing Partial Order Alignments Using Net Unfoldings*. Master’s thesis, Utrecht University (2024)
9. Geurtjens, D.: *Douwegeurtjens/unfolding-alignments: v1.0* (may 2025). <https://doi.org/10.5281/zenodo.15552463>
10. Gianola, A., Montali, M., Winkler, S.: Object-centric conformance alignments with synchronization. In: *CAiSE. LNCS*, vol. 14663, pp. 3–19. Springer (2024)
11. Greco, G., Guzzo, A., Pontieri, L., Saccà, D.: Discovering expressive process models by clustering log traces. *IEEE Trans. Knowl. Data Eng.* **18**(8), 1010–1027 (2006)
12. Leemans, S.J.J., van Zelst, S.J., Lu, X.: Partial-order-based process mining: a survey and outlook. *Knowl. Inf. Syst.* **65**(1), 1–29 (2023)
13. Lu, X., Fahland, D., van der Aalst, W.M.P.: Conformance checking based on partially ordered event data. In: *BPM Workshops. LNBIP*, vol. 202, pp. 75–88. Springer (2014)
14. Lu, X., Mans, R., Fahland, D., van der Aalst, W.M.P.: Conformance checking in healthcare based on partially ordered event data. In: *ETFA*. pp. 1–8. IEEE (2014)
15. Mannhardt, F.: Sepsis cases - event log (2016). <https://doi.org/10.4121/UUID:915D2BFB-7E84-49AD-A286-DC35F063A460>
16. Mannhardt, F., de Leoni, M., Reijers, H.A., van der Aalst, W.M.P.: Balanced multi-perspective checking of process conformance. *Computing* **98**(4), 407–437 (2016)
17. McMillan, K.L.: Using unfoldings to avoid the state explosion problem in the verification of asynchronous circuits. In: *CAV. LNCS*, vol. 663, pp. 164–177. Springer (1992)
18. Munoz-Gama, J., Carmona, J., van der Aalst, W.M.P.: Conformance checking in the large: Partitioning and topology. In: *BPM. LNCS*, vol. 8094, pp. 130–145. Springer (2013)
19. Rozinat, A., van der Aalst, W.M.P.: Conformance checking of processes based on monitoring real behavior. *Inf. Syst.* **33**(1), 64–95 (2008)
20. Siddiqui, A., van der Aalst, W.M.P., Schuster, D.: Computing alignments for partially-ordered traces through petri net unfoldings. *CoRR* **abs/2504.00550** (2025 (April 4))

A Additional Examples

A.1 Partial-order traces

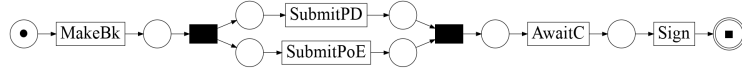


Fig. 13: The partial order trace, converted to an event net.

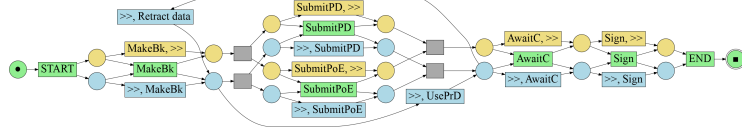


Fig. 14: The synchronous product.

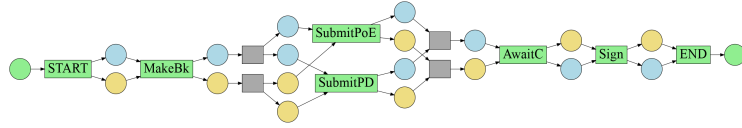


Fig. 15: The unfolding alignment.

A.2 Unbounded, easy sound net

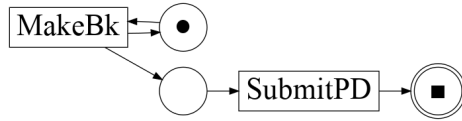


Fig. 16: An unbounded, easy sound net, meaning the final marking is reachable, where the final marking is a token in the initial place and a token in the final place.

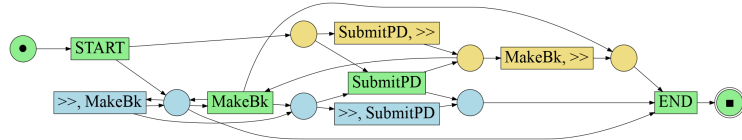


Fig. 17: The synchronous product between the easy sound net and the trace $\sigma = \langle \text{SubmitPD}, \text{MakeBk} \rangle$. Note that we added a dummy start and a dummy end transition to ease the checking of termination conditions.

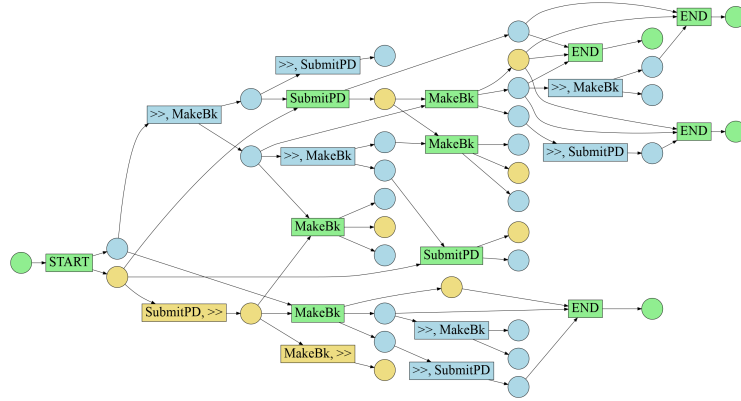


Fig. 18: The directed unfolding, trying to find the target marking.

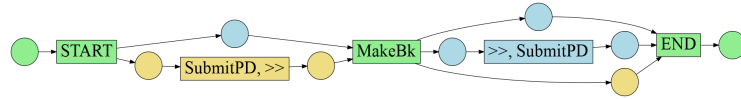


Fig. 19: The final unfolding alignment net.

B Notations

A **multiset** b over A is a function $b : A \rightarrow \mathbb{N}$, which returns the count of element a in multiset b . We use $\mathcal{B}(A)$ for the set of all multisets over a finite domain A . For example, $b_1 = []$ (empty), $b_2 = [x, x, y]$, $b_3 = [x, y, z]$, and $b_4 = [x^3, y^2, z]$ are multisets over $A = \{x, y, z\}$, where order does not matter. Standard set operations extend to multisets, e.g., union ($b_2 \uplus b_3 = b_4$), difference ($b_4 \setminus b_2 = b_3$), and cardinality ($|b_4| = 6$). A multiset b is a subset of b' ($b \leq b'$) if $b(a) \leq b'(a)$ for all $a \in A$, with strict inclusion ($b < b'$) requiring inequality for at least one element.

A **sequence** $\sigma = \langle a_1, a_2, \dots, a_n \rangle$ over X has length $|\sigma|$ and supports concatenation, e.g., $\langle x, x, y \rangle \cdot \langle x, y, z \rangle = \langle x, x, y, x, y, z \rangle$. Sequences can be converted to multisets using $[a \in \sigma]$, e.g., $[a \in \langle x, x, y, x, y, z \rangle] = [x^3, y^2, z]$.

Definition 14 (Petri Net). A Petri Net $N = (P, T, F)$ is a 3-tuple in which P is a set of places, T is a set of transitions, and $F \subseteq (P \times T) \cup (T \times P)$ defines the flow relations. A marking m of N is a multiset of P , i.e., m assigns each place $p \in P$ a number $m(p)$ of tokens and presents a state of the net.

A marked Petri net $N = (P, T, F, i, f)$ is a Petri net with an initial marking i and a final marking f . The preset $\bullet x$ of a node x is the set $\{y \mid (y, x) \in F\}$. Similarly, the postset x^\bullet of a node x is the set $\{y \mid (x, y) \in F\}$.

A transition t of N is enabled at a marking m of N , iff for all $p \in \bullet t$, $m(p) > 0$. If t is enabled at m , then t may fire or occur, and its occurrence leads to a successor marking m' with $m'(p) = m(p) - \bullet t + t^\bullet$. We use $m \xrightarrow{t} m'$ to denote this relation. A sequence $\sigma = \langle t_1, t_2, \dots, t_n \rangle$ of transitions is an occurrence sequence of N

if there exist markings i, m_1, m_2, \dots, m_n such that $i \xrightarrow{t_1} m_1 \xrightarrow{t_2} m_2 \dots \xrightarrow{t_n} m_n$, also denoted by $i \xrightarrow{\sigma} m_n$. A marking m is a reachable marking if there exists an occurrence sequence σ such that $i \xrightarrow{\sigma} m$. A marking M of a net is n -safe if $m(p) \leq n$ for every place $p \in P$. A net is n -safe if all its reachable markings are n -safe. In the following, we assume all nets to be 1-safe nets.

Definition 15 (Causal $<$, conflict $\#$, and concurrency $||$). Given a net, we define the causal, conflict, and concurrency relations between nodes of a net as follows:

- Two nodes x and y are in causal relation, denoted by $x < y$, if the net contains a path with at least one arc leading from x to y .
- x and y are inconflct relation, or just in conflict, denoted by $x \# y$, if the net contains two paths st_1, \dots, x_1 and st_2, \dots, x_2 starting at the same place s , and such that $t_1 = t_2$. In words, x_1 and x_2 are in conflict if the net contains two paths leading to x_1 and x_2 which start at the same place and immediately diverge (although later on they can converge again).
- x and y are in concurrency relation, denoted by $x || y$, if neither $x < y$ nor $y < x$ nor $x \# y$.